Mechanism of reducing force and tillage performance analysis of bionic subsoiler based on discrete element method

Li Bo[1*], Wang Xuewen[1], Xia Rui[1], Chen Jun[2], Yang Zhaojian[1]

(1. *Shanxi Key Laboratory of Fully Mechanized Coal Mining Equipment, Taiyuan University of Technology, Taiyuan 030024, China;*
2. *College of Mechanical and Electronic Engineering, Northwest A & F University, Yangling 712100, China*)

Abstract: Subsoiling is an important part in conservation tillage. However, the large tillage force of subsoilers is one of the existing problems for further promoting. This study compared the tillage forces of a bionic subsoiler and a standard arc-shaped subsoiler using experiments. The tillage velocity was 0.8 m/s and the tillage depth was 220, 260 and 300 mm, respectively. The discrete element model of soil-subsoiler interaction was established and the tillage process was simulated under the same condition with the test. The mechanism of reducing force and tillage performance of the bionic subsoiler were analyzed. Results showed that bionic subsoiler could reduce tillage force significantly and the force reducing rate was 26.81%, 19.97% and 10.99% under the depth of 220, 260 and 300 mm, respectively. The discrete element model could simulate the tillage process well. Soil particles pushed by arc-shaped subsoiler moving towards the center of the arc and the subsoiler's lifting effect on the soil were the two reasons of arc-shaped subsoiler's larger force. The tillage performance of these two subsoilers was almost the same.

Keywords: bionic subsoiler, reducing force, tillage performance, DEM, PFC^{3D}

Citation: Li, B., X. W. Wang, R. Xia, J. Chen, and Z. J. Yang. 2017. Mechanism of reducing force and tillage performance analysis of bionic subsoiler based on discrete element method. International Agricultural Engineering Journal, 26(3): 27–36.

1 Introduction

As the main conservation tillage component, subsoiler is used for loosing soil without disturbing the soil layer. During the working process, the subsoiler cuts and breaks the soil by the shank and the point. Therefore, the structure of the subsoiler has direct impacts on tillage force and the whole machine performance. However, the subsoiler has the problem of large energy consumption, which hindered further promoting of the deep loosing technology.

Different methods have been tried to achieve the purpose of reducing the resistance of tillage components. Some scholars reduced the tillage force by adding vibration on working parts. Shahgoli et al. (2010) studied the vibration subsoiler and found that the tillage force could be reduced from 25.8 kN to 9.3 kN as the vibration frequency changing between 1.9 Hz and 8.8 Hz comparing with the original subsoiler. Mouazen and Nemenyi (1999a; 1999b) and Mouazen (1999) predicted the tillage force of four kinds of subsoiler using the finite element method (FEM). Results showed that the subsoiler had the minimum tillage force as the shank had an angle of 75° combining with a rake angle of 15°, which achieved the required tillage performance. Mouazen and Ramon (2002) used a regression equation to analyze the tillage force under different moisture contents, bulk densities and working depths. Abo-Elnor (2004) studied the bulldozing plate and found that the width of bulldozing plate had great influence on the tillage force, which provided ideas for optimizing tillage machinery.

The structure of existing animals has adapted to the environment in the long process of evolution, and animal structures provide the basis for human bionic researches. Many applications have been tried in improving agricultural machinery using bionic methods (Ren et al., 2006). To improve the wear resistance of soil engaging tools, the texture of shell surface was applied by Tong et

Received date: 2017-02-09 **Accepted date:** 2017-06-26

* **Corresponding author: Li Bo,** Shanxi Key Laboratory of Fully Mechanized Coal Mining Equipment, Taiyuan University of Technology. Email: libo@tyut.edu.cn.

al. (2010). Less pressure was found on opener surface after applying the convex domes of beetles (Tong et al., 2009). The structure of mole claw was used to reduce the resistance of soil cutting tools (Ji et al., 2010; Zhang et al., 2016). The claw of animals good at burrowing (like pangolin, rat, rabbit, bear) had evolved into the structure suitable for interacting with soil. During the working process, the subsoiler can loose soil, break the plow pan, so as to improve the water storage capacity of soil and the growth condition of plants. Therefore, the application of the claw's structure in optimizing the subsoiler would solve the problem of large tillage force. Guo et al. (2010) compared the tillage performance of tillage tools' soil contacting line applying on the claw of rat, vole, mole cricket and rooster. Results showed that the soil contacting line and longitudinal/depth ratio were the two important factors affecting the tillage force. The curved tillage tools obtained better tillage performance compared with linear ones under the small longitudinal/depth ratio (less than 1); parabolic tillage tools could obtain good mechanical properties of tillage in a wide range of longitudinal/depth ratio; cycloid curve was suitable for designing tillage part with larger longitudinal/depth ratio (more than 2). Guo et al. (2003) also found that the best cutting performance occurred when the longitudinal/depth ratio was between 0.6 and 0.9. Zhu and Tong (2003) described the application of effective and energy-saving subsoiling technology, and predicted the bionic subsoiler development trend. The above studies provided the research foundation of bionic applications on subsoiler design. Bear is good at digging holes using its sharp and curved claw, the shape of which is suitable for designing subsoilers. Thus, this study analyzed a bionic subsoiler based on the bear claw for the purpose of reducing tillage force.

In recent years, the DEM has been widely used in agricultural engineering, mainly in optimizing agricultural machine and some basic soil engaging experiments (Li et al., 2014; Sun et al., 2009). Many scholars studied the soil-tool interaction using the DEM (Ucgul et al., 2017). Tsuji et al. (2012) used the bond model (Utili and Nova, 2008) to analyze the working process of bulldozing plate. The cohesive force between particles had significant influence on particles' motion and the bulldozing resistance increased as the bond strength increased. Momozu et al. (2002) simulated the soil breaking process under the effect of soil cutting tools. The discrete element model was established by adding bonds between particles to reflect the real process of loosing soil better. Shmulevich et al. (2007) used the method proposed by Asaf et al. (2007) to determine the parameters of soil particles. The tillage forces of four kinds of tools were compared and the soil movement was also analyzed. However, this particle model was established by two-dimensional disk, which had a certain gap with actual particles. Van der Linde (2007) analyzed the tillage force and working performance of vibration subsoilers under different frequencies using the DEM. The reasons of reducing force by vibration were also analyzed. Shmulevich (2010) analyzed applications of the DEM in studying the soil-tool interaction and pointed out the advantages and limitations by using this method.

Above studies showed that some scholars designed the bionic subsoiler and achieved good experimental results. However, the movement of soil particles during the soil-subsoiler interaction and the reasons of bionic subsoiler's reducing force have not been analyzed using DEM. In this study, the DEM was used to establish a soil-subsoiler interaction model. The purposes of this study were: 1). explaining the reasons of bionic subsoiler's reducing force comparing with the arc-shaped subsoiler (JB/T 9788-1999); 2). analyzing the tillage performance of the bionic subsoiler using DEM.

2 Methodology

2.1 Theoretical force analysis

The point of the subsoiler could be regarded as the horizontal low speed movement of a slope in the soil during the tillage. Soehne (1956) analyzed the interaction between the soil and the point. The forces applied on the soil block above the point are shown in Figure 1. Shear failure occurred in front of the point during the process of cutting soil. Gravity, acceleration force, friction were acted on the soil block above the point. For no stone and other debris in the soil, the cutting resistance could be neglected.

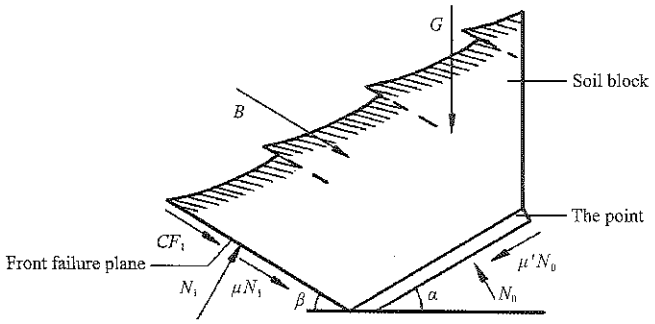

Figure 1 Force applied on the soil block

Through the above analysis of force, force balance equations of soil block above the point in horizontal and vertical direction could be listed as follows:

For horizontal direction:

$$N_0(\sin\alpha+\mu'\cos\alpha)-N_1(\sin\beta+\mu\cos\beta)-(CS'+B)\cos\beta=0 \quad (1)$$

For vertical direction:

$$N_0\cos\alpha-\mu'N_0\sin\alpha+N_1\cos\beta-(B+CS'+\mu N_1)\sin\beta-G=0 \quad (2)$$

where, N_0 is pressure from the soil block above the point (N); μ' is friction coefficient between soil and metal; α is rake angle (°); N_1 is pressure from the front failure surface (N); β is the angle between the front failure surface and horizontal direction (°); B is acceleration force of the soil block above the point (N); C is cohesion of soil (Pa); S' is the area of the front failure surface (m^2); μ is friction coefficient between soil particles, and G is the weight of soil above the point (kg).

The cutting ability is the main function of the shank. Figure 2 shows the force acting on the shank. Three main parts of force were acted on the shank: the force components caused by the normal force applied on the wedge edge, the force components caused by the tangential force applied on the wedge edge, and the force components caused by the tangential force applied on the side face. Therefore, the force of soil applied on the shank could be expressed as follows:

$$W=2\left(N_2\sin\frac{\varphi'}{2}+N_2\mu'\cos\frac{\varphi'}{2}+N_3\mu'\right) \quad (3)$$

where, W is the total force acted on the shank in the horizontal direction, N; φ' is the angle of the wedge edge, °; N_2 is the normal force acted on the wedge edge, N; and N_3 is the normal force acted on the side face, N.

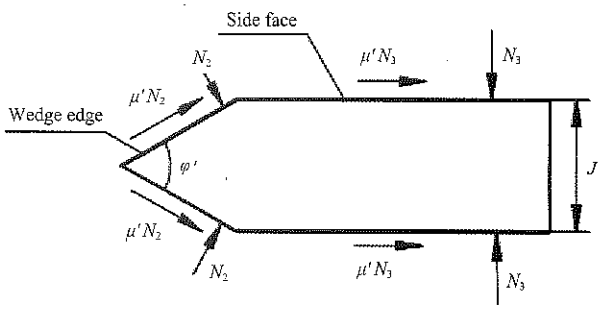

Figure 2 Force applied on the shank

2.2 Subsoilers used in the test

The bionic subsoiler tested in this study was designed based on the standard arc-shaped subsoiler and the curve of bear claw (Li et al., 2015).

Three subsoilers were tested, in which, S_1 is the bionic subsoiler shank with chisel-shaped point; S_2 is the bionic subsoiler; S_3 is the standard arc-shaped subsoiler. S_1 and S_2 had the same shank, while S_1 and S_3 had the same point. The soil bin test was completed in the agriculture machinery lab, i.e. Northwest A&F University, Yangling, Shaanxi, China. The soil type was sandy loam soil.

Figure 3 shows the bionic subsoiler S_2 and the standard arc-shaped subsoiler S_3. Figures 3b and 3d were the bionic point and the standard chisel point, respectively. S_1 was the subsoiler of S_2 replaced by the standard chisel point. The subsoiler was fixed on the working frame by a U shaped clip. Keep the working frame in horizontal position by adjusting the three point suspension device. By using the hydraulic lift system, the subsoiler work was set at the specified tillage depth and the velocity of 0.8 m/s. Make sure the data acquisition system work well before running the traction wagon. The working depth of the subsoiler was 220, 260 and 300 mm, respectively. The soil should be leveled and compacted after each test and make sure the rigidity maintain the same. Each test was repeated three times and the average value was taken as the final results.

2.3 Soil preparation and the test

(1) Soil watering

To achieve similar soil moisture with the field, soil in the soil bin needed to be watered by the watering system of the traction wagon. Two weeks of natural infiltration were required to avoid the moisture content of upper soil higher than the lower part. The soil moisture content was

monitored from the depth of 220 mm to 300 mm until it reached 19.0%.

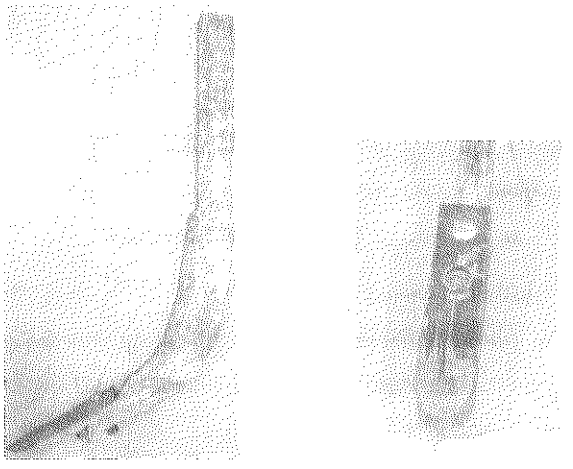

a. Bionic subsoiler b. Bionic point

c. Standard arc-shaped subsoiler d. Standard chisel point

Figure 3 Bionic subsoiler and standard subsoiler

(2) Rotary tilling and soil leveling

The soil surface was not smooth enough when the soil reached the specified soil moisture. What's worse, some large clods were still existed. Therefore, the clods should be broken and the land should be leveled. The rotary cultivator was hung on the traction wagon to break the clods and a scraper plate was used to level the soil (Figure 4a).

(3) Soil compaction

The soil was relatively flat after rotary tillage, and the soil compaction was required to reach the soil compactness in the field. A rolling wheel of 1.2 t was hung on the traction wagon to compact the soil (Figure 4b).

(4) Soil rigidity measurement

Soil rigidity was measured after soil compaction to ensure the consistent soil compactness (Figure 4c). Probe test was carried out at 10 positions in the travelling direction of the subsoiler. The average value of 10 points was taken as the soil rigidity (460 kPa).

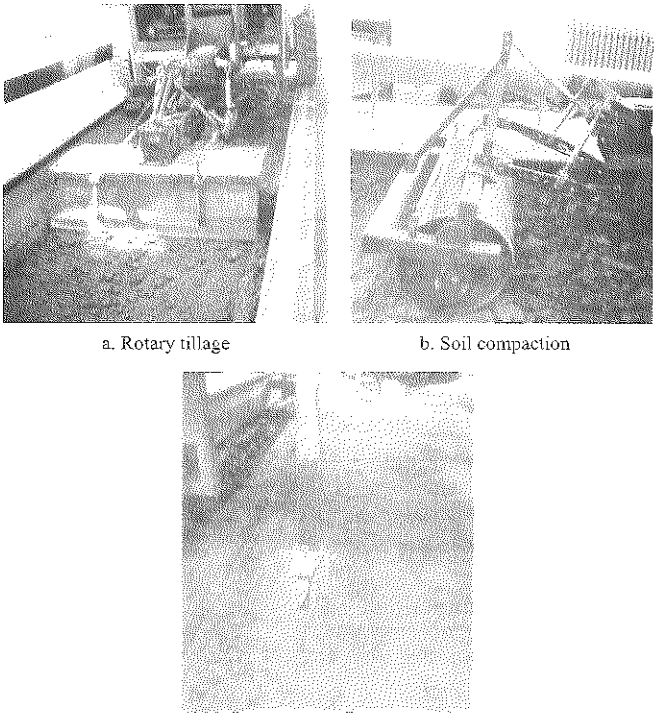

a. Rotary tillage b. Soil compaction

c. Soil compaction test

Figure 4 Preparation of soil bin test

Subsoiler of S_1, S_2 and S_3 was hung on the traction wagon respectively (Figure 5). The travelling velocity of each subsoiler was 0.8 m/s. After each test, the soil should be leveled and compacted for next test. The horizontal resistance of each subsoiler was monitored by sensors during the test. The upper link sensor, hanging pin sensor and angle sensor transferred the measured data to the dynamic data collector. The draft force was the horizontal vector sum of these forces. The data collector sent the data through the antenna to a laptop which would finally deal with the data. The tillage length of each subsoiler was 22 m, and the tillage force was taken from the stable working area of 3 m to 18 m from the start position.

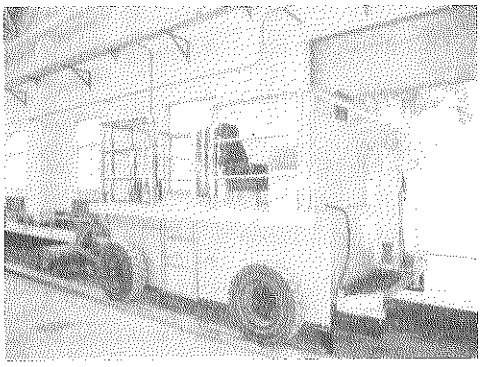

Figure 5 The four-wheel-drive soil bin traction wagon

2.4 The DEM parameters

The soil bin (1 m long, 0.5 m wide and 1 m high) with five walls was established by PFC^{3D}. The soil used in the test was a kind of sandy loam soil and the liquid bridge force between soil particles should be considered. Therefore, the parallel bonds were added to soil particle model using DEM. The DEM parameters of soil used in the simulation were adjusted by comparing the simulation results with the laboratory triaxial compression test. The soil used for the triaxial compression test was the same with the one used in the tillage test. Set the minimum radius of the soil particle to 0.6 mm and the ratio of maximum/minimum radius to 3:1. The soil porosity was same with the soil test (0.4). The DEM parameters for the simulation are listed in Table 1.

Table 1 Parameters for DEM simulation

Parameter	Value
Soil porosity	0.40
Friction factor	0.93
Soil particle density, kg/m^3	2760
Particle-particle contact normal stiffness, N/m	4×10^5
Particle-particle contact shear stiffness, N/m	3.5×10^5
The critical damping ratio in the normal direction	0.8
The critical damping ratio in the shear direction	0.6
The parallel-bond radius multiplier	1.0
The parallel-bond normal stiffness, Pa/m	4×10^5
The parallel-bond shear stiffness, Pa/m	4×10^5
The parallel-bond normal strength, Pa	4×10^5
The parallel-bond shear strength, Pa	4×10^5

Different structures of subsoiler would lead to different forms of soil movement. To analyze the soil movement clearly, two layers of green belt, 75 mm in thickness, were applied in the simulation (Figure 6). Only the color of these two layers was different from other soil particles, soil properties maintained the same. The working condition of the simulation was the same with the test.

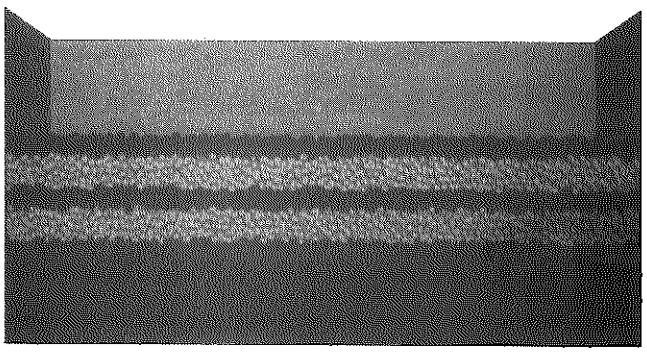

Figure 6 The initial state of the soil

3 Results and discussion

3.1 Tillage resistance

Figure 7 shows the horizontal resistance curve of S_1, S_2, S_3 during the stable state under the working depth of 260 mm. The tillage forces of S_1, S_2 and S_3 were F_{21}, F_{22}, and F_{23}, respectively. It showed that the tillage force fluctuated around the mean value. The tillage force had great volatility in the test, which was caused by the inhomogeneity of soil conditions and the clods in the soil bin. The green curve represented the force of standard arc-shaped subsoiler (S_3), which was relatively higher than other two and the fluctuation range was the maximum among these three curves. The bionic subsoiler (S_2) was the blue curve, which had the lowest tillage force and the smallest fluctuation, indicating the bionic subsoiler could effectively reduce tillage resistance and operate stably. The red curve fluctuated greatly and the tillage force was between the other two.

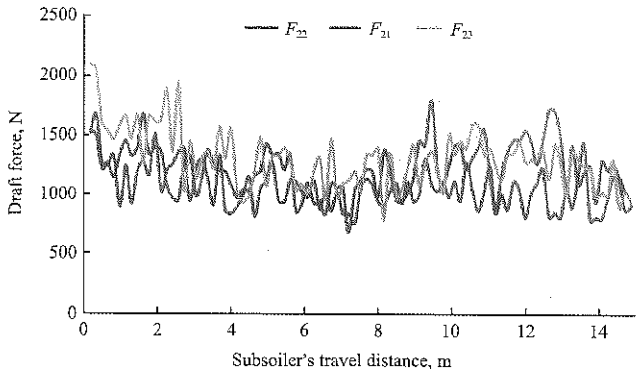

Figure 7 The horizontal resistance of three subsoilers in the test (depth is 260 mm)

The simulation and test results of three kinds of subsoiler under 0.8 m/s are listed in Table 2. The F_{11}, F_{12} and F_{13} were the simulation results of S_1, S_2 and S_3, respectively. The F_{21}, F_{22} and F_{23} were the tillage resistance of the test that corresponding to simulation. The ε was the force reducing rate of S_2 relative to S_3 in simulation; δ was the corresponding reducing rate in the test. θ_1, θ_2 and θ_3 were the simulation relative errors of S_1, S_2 and S_3 respectively, comparing with the test.

The S_3 had the largest tillage resistance, and S_2 had the smallest resistance at the velocity of 0.8 m/s under three depths (Table 2). The DEM simulation achieved the similar results. The relative errors were between 1.42% and 27.43%, which were in the allowable range,

indicating that the DEM could predict the tillage force of a subsoiler instead of doing experiments. The relative errors larger than 20% only happened at the depth of 220 mm for S_2, which required further analysis.

Table 2 The tillage resistance results of three subsoilers

Depth, mm	F_{11}, N	F_{12}, N	F_{13}, N	F_{21}, N	F_{22}, N	F_{23}, N	ε, %	δ, %	θ_1, %	θ_2, %	θ_3, %
220	1042	929	1055	869	729	996	11.94	26.81	19.91	27.43	5.92
260	1199	1124	1310	1234	1074	1342	14.20	19.97	2.84	4.66	2.38
300	1566	1521	1615	1544	1491	1675	5.82	10.99	1.42	2.01	3.58

3.2 Force reducing mechanism and tillage performance of the bionic subsoiler

3.2.1 Soil disturbance analysis

To compare the soil disturbances of bionic subsoiler and the standard arc-shaped one working at different stages, the soil was cut in the travelling direction (Figure 8). Based on the travelling stage of the subsoiler, three distances of 250, 350 and 600 mm from the start position were selected, respectively. In the first stage, the point and parts of the shank entered into the soil bin; in the second stage, the inner baseline of two subsoilers entered into the soil bin; in the third stage, two subsoilers worked in the stable stage. The velocity field, the contact force field and the parallel bond field were all compared in these three stages.

The soil in front part of the subsoiler was lifted when the subsoiler entered into the soil bin (Figures 8a and 8d). More soil disturbance and fluctuation were observed as the subsoiler entering into the soil (Figures 8b and 8e). In the stable stage, soil around the point suffered more disturbance than other areas (Figures 8c and 8f), which meant the point of the subsoiler had the function of breaking plow pan. These two subsoilers were similar in soil disturbance.

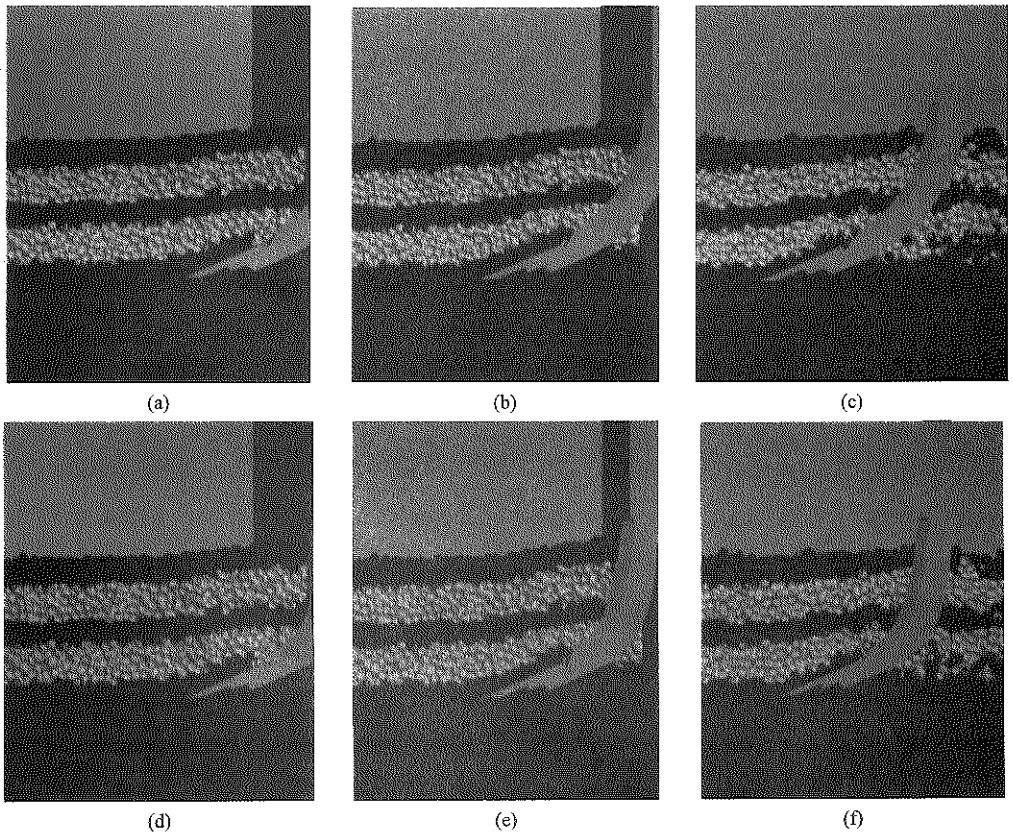

Figure 8 Dynamic behaviors of soil particles

(a)-(c) Standard arc-shaped subsoiler; (d)-(f) Bionic subsoiler

3.2.2 Velocity field analysis

The velocity field of the disturbed soil particles could be reflected by different colors during the simulation. Figure 9 is the velocity contour. The direction of each particle's velocity could be reflected by the arrow while the length of the arrow showed the magnitude.

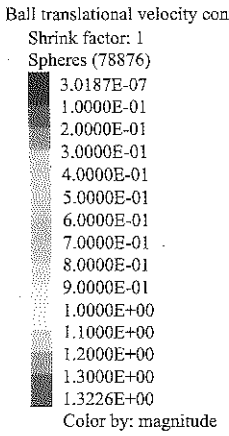

Figure 9 Velocity contour

As the subsoiler travelling into the soil bin, the disturbed area increased gradually until the whole subsoiler entered into the soil (Figure 10). Soil particles started to move under the effect of the point in the first stage (Figures 10a and 10d). The difference was obvious in the second stage. Soil particles pushed by the arc-shaped subsoiler moving towards the center of the arc. This would lead to the accumulation of soil and hindered the subsoiler travelling forward (Figure 10b). While soil moved in the direction of inclining upward under the effect of bionic subsoiler (Figure 10e). During the stable stage (Figures 10c and 10f), more soil was thrown behind the arc-shaped subsoiler with relatively higher velocity compared with the bionic subsoiler. It could be explained that arc-shaped subsoiler had more lifting effect on the soil. However, large lifting effect was useless for improving the tillage performance and would increase the tillage resistance and the surface roughness. For the purpose of tillage was loosening the soil and the plow pan without disturbing land layers. In addition, the rough soil surface was helpless for the subsequent field work.

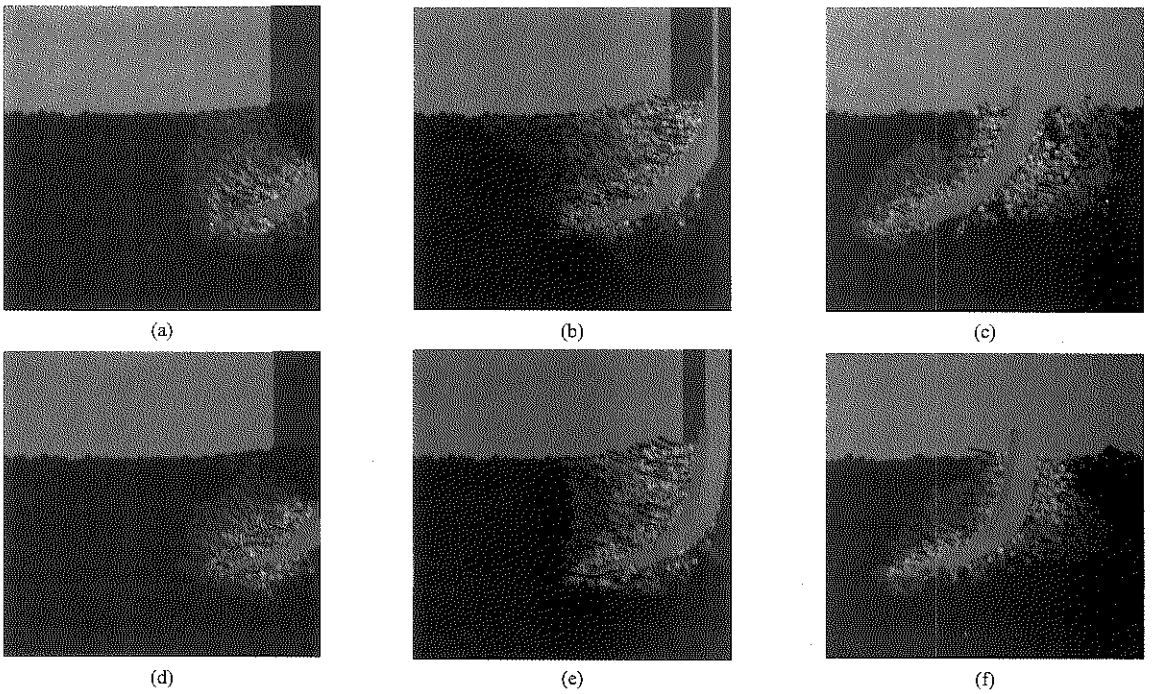

Figure 10 Velocity field

(a)-(c) standard arc-shaped subsoiler; (d)-(f) bionic subsoiler

3.2.3 Contact force field

Contact force between particles was formed at the contact point in PFC^{3D} (Itasca 2015). The contact force field was composed by the force chain whose size reflected the magnitude of force. The force chain would break when the force acting on soil particles exceeded the contact force. In this study, the contact force field was obtained from the 42 mm thick slice containing the subsoiler (Figure 11), so that the force chain around the subsoiler could be reflected.

Figure 11 showed that the contact force mainly concentrated at the contact surface of the subsoiler. For these two subsoilers, the point suffered larger concentrated force than other parts. From the analysis of three stages, the stress concentration areas were basically the same: the upper surface of the point and the edge of the shank. The force chains between soil particles were broken after tillage (Figures 11c and 11f). There was almost no difference in breaking the force chain, which showed that these two subsoilers had similar tillage performance.

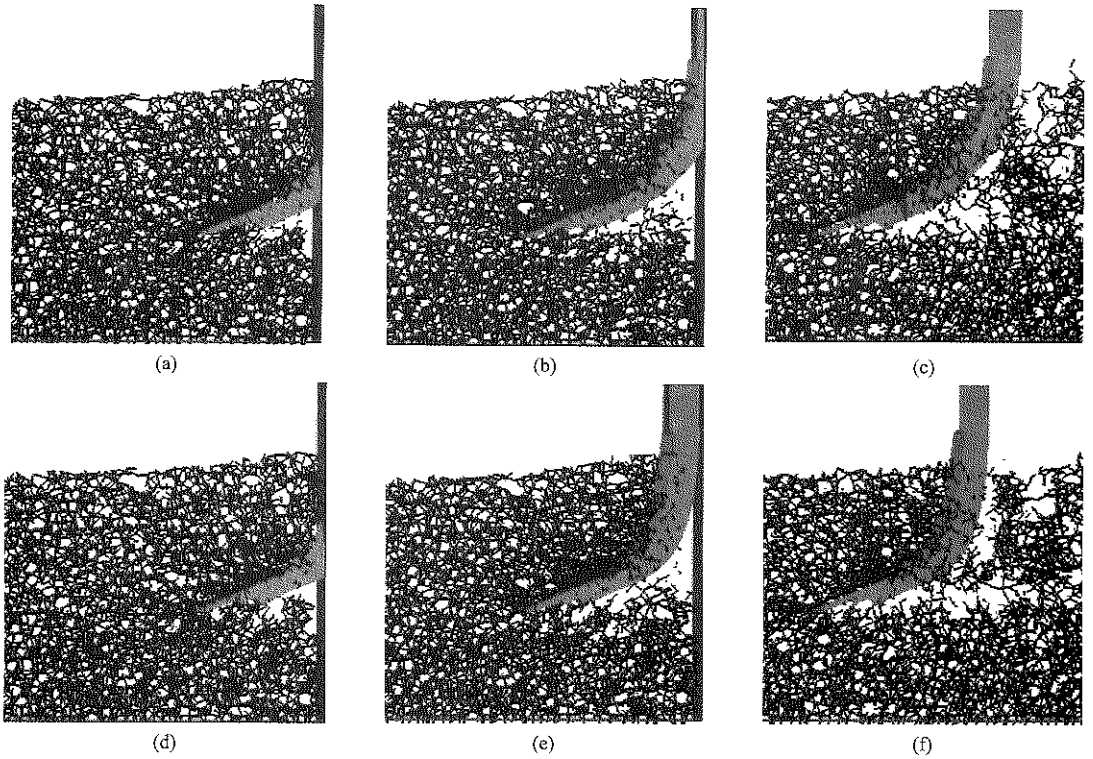

Figure 11 Contact force field

(a)-(c) Standard arc-shaped subsoiler; (d)-(f) Bionic subsoiler

3.2.4 Parallel bond field

Parallel bonds were the cylindrical areas between two contact soil particles to bear the force and torque. Parallel bonds around the point were broken as the subsoiler entered into the soil bin (Figures 12a and 12d). More bonds were destroyed as the subsoiler moving forward (Figures 12b and 12e). The bond chains behind the subsoiler became sparse for the contact soil particles were disturbed. Two subsoilers had the similar effect on disturbing the soil.

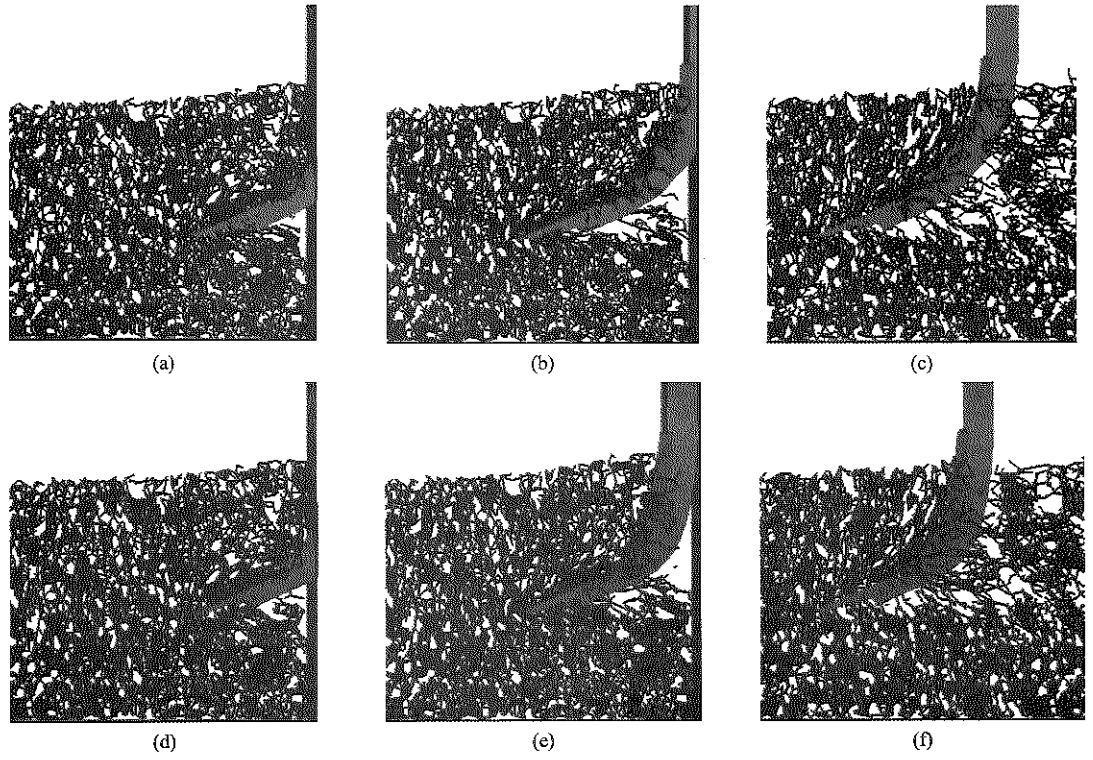

Figure 12 Parallel bond field

(a)-(c) Standard arc-shaped subsoiler; (d)-(f) Bionic subsoiler

In summary, two subsoilers were similar in tillage performance after comparing them in soil movement, velocity field, force field and parallel bond field.

4 Conclusions

This study compared the bionic subsoiler and the standard arc-shaped subsoiler by the DEM simulation and soil bin test. Results showed that the bionic subsoiler could reduce the tillage force significantly. By comparing these two subsoilers in soil movement, velocity field, contact force field and parallel bond field, the mechanism of reducing tillage force and the tillage performance were analyzed. Results showed that soil particles moving towards the center of the arc and the high lifting effect were the reasons of arc-shaped subsoiler's large tillage force. The bionic subsoiler had the similar tillage performance in disturbing the soil and breaking the contacts with the standard arc-shaped subsoiler. This study explained the reasons of reducing force using the bionic subsoiler and provided the theoretical basis for designing subsoilers. It should be noticed that the above conclusions were drawn for a specific soil (sandy loam soil) in the given soil moisture content. For different conditions, further research is required.

Acknowledgment

The project was supported by the Open Research Fund of Shanxi Key Laboratory of Fully Mechanized Coal Mining Equipment (No. mkzczb201602), Youth Foundation of Taiyuan University of Technology (No. 1205-04020203).

[References]

[1] Abo-Elnor, M., R. Hamilton, and J. T. Boyle. 2004. Simulation of soil-blade interaction for sandy soil using advanced 3D finite element analysis. *Soil & Tillage Research*, 75(1): 61–73.

[2] Asaf, Z., D. Rubinstein, and I. Shmulevich. 2007. Determination of discrete element model parameters required for soil tillage. *Soil & Tillage Research*, 92(1-2): 227–242.

[3] Guo, Z. J., D. Y. Zhou, and Z. L. Zhou. 2010. Simulation research on mechanical performances of several kinds of cultivating components with different soil-engaging surfaces. *Journal of Mechnical Engineering*, 46(15): 71–75.

[4] Guo, Z. J., and Z. L. Zhou. 2003. 2D Finite element analysis for the cutting performance of bionic curved cutting tools. *Chinese Journal of Mechanical Engineering*, 39(9): 106–109.

[5] Itasca. 2015. PFC3D-Particle flow code in three dimensions, theory and background. Itasca Consulting Group, Inc., Minneapolis, MN, USA.

[6] JB/T 9788-1999. 2000. Subsoiler and share shaft. Machinery Industry Standard of the People's Republic of China.

[7] Ji, W. F., D. H. Chen, H. L. Jia, and J. Tong. 2010. Experimental investigation into soil-cutting performance of the claws of mole rat (*Scaptochirus moschatus*). *Journal of Bionic Engineering*, 7(3): S166–S171.

[8] Li, B., F. Y. Liu, J. Y. Mu, J. Chen, and W. T. Han. 2014. Distinct element method analysis and field experiment of soil resistance applied on the subsoiler. *International Journal of Agricultural and Biological Engineering*, 7(1): 54–59.

[9] Li, B., F. Y. Liu, R. Xia, and J. Chen. 2015. Distinct element method analysis and experiment of a biomimetic subsoiler. *International Agricultural Engineering Journal*, 24(1): 47–54.

[10] Momozu, M., A. Oida, M. Yamazaki, and A. J. Koolen. 2002. Simulation of a soil loosening process by means of the modified distinct element method. *Journal of Terramechanics*, 39(4): 207–220.

[11] Mouazen, A. M., and M. Nemenyi. 1999a. Finite element analysis of subsoiler cutting in non-homogeneous sandy loam soil. *Soil & Tillage Research*, 51(1-2): 1–15.

[12] Mouazen, A. M., and M. Nemenyi. 1999b. Tillage tool design by the finite element method: part 1. finite element modelling of soil plastic behaviour. *Journal of Agricultural Engineering Research*, 72(1): 37–51.

[13] Mouazen A. M., M. Nemenyi, H. Schwanghart., and M. Rempfer. 1999. Tillage tool design by the finite element method: part 2. experimental validation of the finite element results with soil bin test. *Journal of Agricultural Engineering Research*, 72(1): 53–58.

[14] Mouazen, A. M., and H. Ramon. 2002. A numerical-statistical hybrid modelling scheme for evaluation of draught requirements of a subsoiler cutting a sandy loam soil, as affected by moisture content, bulk density and depth. *Soil & Tillage Research*, 63(3-4): 155–165.

[15] Ren, L. Q., Z. W. Han, J. Q. Li, and J. Tong. 2006. Experimental investigation of bionic rough curved soil cutting blade surface to reduce soil adhesion and friction. *Soil & Tillage Research*, 85(1-2): 1–12.

[16] Shahgoli, G., J. Fielke, J. Desbiolles, and C. Saunders. 2010. Optimising oscillation frequency in oscillatory tillage. *Soil & Tillage Research*, 106(2): 202–210.

[17] Shmulevich, I. 2010. State of the art modeling of soil-tillage interaction using discrete element method. *Soil & Tillage*

Research, 111(1): 41–53.

[18] Shmulevich, I., Z. Asaf, and D. Rubinstein. 2007. Interaction between soil and a wide cutting blade using the discrete element method. *Soil & Tillage Research*, 97(1): 37–50.

[19] Soehne, W. 1956. Some principles of soil mechanics as applied to agricultural engineering. *Grundlagen der Landtechnik*, 7: 11–27.

[20] Sun, P., F. Gao, W. Li, S. Z. Yao, and Y. T. Gong. 2009. Discrete element simulation of cone penetration process. *Transactions of the CSAM*, 40(1): 184–188.

[21] Tsuji, T., Y. Nakagawa, N. Matsumoto, Y. Kadono, T. Takayama, and T. Tanaka. 2012. 3-D DEM simulation of cohesive soil-pushing behavior by bulldozer blade. *Journal of Terramechanics*, 49(1): 37–47.

[22] Tong, J., B. Z. Moayad, Y. H. Ma, J. Y. Sun, D. H. Chen, H. L. Jia, and L. Q. Ren. 2009. Effects of biomimetic surface designs on furrow opener performance. *Journal of Bionic Engineering*, 6(3): 280–289.

[23] Tong, J., M. A. Mohammad, J. B. Zhang, Y. H. Ma, B. J. Rong, D. H. Chen, and C. Menon. 2010. DEM numerical simulation of abrasive wear characteristics of a bioinspired ridged surface. *Journal of Bionic Engineering*, 7(2): 175–181.

[24] Ucgul, M., C. Saunders, and J. M. Fielke. 2017. Discrete element modelling of tillage forces and soil movement of a one-third scale mouldboard plough. *Biosystems Engineering*, 155: 44–54.

[25] Utili, S., and R. Nova. 2008. DEM analysis of bonded granular geomaterials. *International Journal for Numerical and Analytical Methods in Geomechanics*, 32(17): 1997–2031.

[26] Van der Linde, J. 2007. Discrete element modeling of a vibratory subsoiler. M.S. Thesis. Department of Mechanical and Mechatronic Engineering, University of Stellenbosch, Matieland, South Africa.

[27] Zhang, Z. J., H. L. Jia, and J. Y. Sun. 2016. Review of application of biomimetics for designing soil-engaging tillage implements in Northeast China. *International Journal of Agricultural and Biological Engineering*, 9(4): 12–21.

[28] Zhu, F. W., and J. Tong. 2003. Development of high-efficient and energy-saving bionic bubsoiling techniques. *Journal of Jilin University (Engineering and Technology Edition)*, 33(2): 95–99.